Effect of nickel precursor on the catalytic performance of Ni/Al$_2$O$_3$ catalysts in the hydrodechlorination of 1,1,2-trichloroethane

Pil Kim, Heesoo Kim, Ji Bong Joo, Wooyoung Kim, In Kyu Song, Jongheop Yi [*]

School of Chemical and Biological Engineering, Institute of Chemical Processes, Seoul National University, Shinlim-dong, Kwanak-ku, Seoul 151-744, South Korea

Abstract

Ni catalysts supported on γ-Al$_2$O$_3$ were prepared using three different precursors, nickel nitrate (Ni-N), nickel chloride (Ni-Cl), and nickel sulfate (Ni-S), in an attempt to investigate the effect of metal precursor on the catalytic performance in the hydrodechlorination of 1,1,2-trichloroethane (TCE). It was found that the physicochemical properties of the supported Ni catalysts were different depending upon the identity of Ni precursor. The Ni-Cl catalyst retained nickel oxide and nickel aluminate species that interacted weakly and strongly, respectively, with the alumina support. After reduction, the Ni-Cl catalyst contained relatively large nickel particles and showed a lower initial conversion than the Ni-N catalyst. On the other hand, sulfur species in the Ni-S catalyst were retained, in the form of nickel sulfate and nickel sulfide after calcination and reduction, respectively. Hydrogen adsorption on Ni surface was partially hindered by the sulfur species in the Ni-S catalyst, resulting in the lowest initial activity of Ni-S catalyst among others. After a period of catalytic reaction, the Ni-N catalyst showed the lowest TCE conversion due to the drastic deactivation caused by the interaction between HCl and metallic nickel. The Ni-Cl and Ni-S catalysts were relatively resistant against deactivation, because large nickel particles with a nickel aluminate structure in the Ni-Cl catalyst and highly dispersed sulfur species in the Ni-S catalyst prevented from strong interaction between HCl and metallic nickel. Among the catalysts tested, the Ni-S catalyst experienced the lowest catalyst deactivation and showed the highest vinyl chloride monomer (VCM) yield in the long run.
© 2006 Elsevier B.V. All rights reserved.

Keywords: Nickel precursor; Supported nickel catalyst; Alumina support; 1,1,2-Trichloroethane (TCE); Hydrodechlorination

1. Introduction

Chlorinated organic wastes, which are generated as by-products in the petroleum industry, are very harmful to human beings from an environmental point of view [1,2]. Many efforts have been made to remove the chlorinated organic wastes through incineration [3–6] and catalytic dechlorination [7–13]. Although the incineration process is a well-established and expedient method for the elimination of chlorinated organic wastes, more toxic compounds such as dioxins can be formed [3,4]. Compared to the incineration process, the hydrogen-assisted catalytic dechlorination, known as hydrodechlorination, has been accepted as an attractive method, because the catalytic process can be conducted at low temperatures and can produce valuable products such as olefins and partially chlorinated olefins directly [14–16].

The hydrodechlorination of chlorinated alkanes over supported Ni catalysts has been widely studied by many researchers. Choi and Lee [14,15] reported that high selectivity for propylene could be obtained with Ni/SiO$_2$ in the hydrodechlorination of 1,2-dichloropropane. Another research group [7] investigating the dehalogenation of cyclohexyl chloride over supported Ni catalysts reported that unsaturated hydrocarbon such as cyclohexene was formed via dehydrochlorination. The Ni catalysts used in the hydrodechlorination of chlorinated organic compounds have been typically supported on silica [17,18] or zeolite [19], while studies on the hydrodechlorination of chlorinated organic compounds over Ni/Al$_2$O$_3$ catalysts are limited [20].

One of the major problems in the practical application of hydrodechlorination is the catalyst deactivation. Two factors have been considered to be the main reasons for catalyst deactivation; one is a coke deposition on the metal surface [20–22] and the other is an interaction between metal and HCl. The lat-

[*] Corresponding author. Tel.: +82 2 880 7438; fax: +82 2 888 7295.
  E-mail address: jyi@snu.ac.kr (J. Yi).

ter eventually leads to the transformation of active metal into inactive metal chloride [12,18,23–27]. Since fundamental studies on the catalyst deactivation processes are very limited and reaction conditions examined in many studies are different, it is difficult to generalize that the catalyst deactivation solely results from one of the above two factors. In the case of supported Ni catalysts, however, it has been generally accepted that the catalyst deactivation was mainly due to $NiCl_2$ formed during the reaction [14,15,24–27].

It is well known that the catalytic properties of supported metal catalysts are affected by several factors such as the method of catalyst preparation [28,29], the nature of support [30,31], and the identity of metal precursor [32,33]. However, very limited progress has been made on the issue of metal precursors [32,33].

In this work, nickel catalysts supported on γ-Al_2O_3 were prepared using three types of nickel precursor, nickel nitrate (Ni-N), nickel chloride (Ni-Cl), and nickel sulfate (Ni-S), to elucidate the effect of nickel precursor on the catalytic performance and the deactivation behavior of Ni/γ-Al_2O_3 catalysts in the hydrodechlorination of 1,1,2-trichloroethane (TCE). To our knowledge, this is the first example showing the effect of nickel precursor on the catalytic performance of supported nickel catalysts in the hydrodechlorination reaction.

2. Experimental

2.1. Catalyst preparation

Nickel catalysts supported on γ-Al_2O_3 (Degussa) were prepared by an impregnation method using nickel nitrate (Fluka), nickel chloride (Fluka), and nickel sulfate (Fluka) as a nickel source. Slurry of nickel precursor and alumina support was dried overnight at 120 °C, and it was then calcined at 550 °C for 6 h in a stream of air. The supported catalysts prepared using nickel nitrate, nickel chloride, and nickel sulfate precursors were denoted as Ni-N, Ni-Cl, and Ni-S, respectively. ICP-AES analyses revealed that the nickel loadings were 8.8, 8.7, and 8.4 wt.% for Ni-N, Ni-Cl, and Ni-S, respectively.

2.2. Characterization

Crystalline phases of the calcined and reduced catalysts were identified by X-ray diffraction using Cu Kα radiation (XRD, M18XHF-SRA, MAC/Science). Surface area and pore volume of the supported Ni catalysts were determined from nitrogen adsorption isotherms at 77 K using ASAP 2010 instrument (Micromeritics). Metallic states of Ni species were confirmed by ultra violet diffuse reflectance spectroscopy (UV-DRS, Perkin-Elmer, Rambda-20 spectrometer) within a range of 300–800 nm. To obtain surface information of the catalysts, X-ray photoelectron spectroscopy (XPS) measurements were done with an AXIS-HS equipment. The binding energies were calibrated with respect to carbon species (C 1s at 284.6 eV). Hydrogen chemisorption measurements were carried out in a conventional chemisorption unit. Each catalyst sample (0.5 g) was placed in a glass sample holder, and was then reduced with hydrogen at 500 °C for 6 h. The sample was evacuated for 1 h

at 500 °C, and then cooled down to room temperature under vacuum. Isotherms for total and irreversible hydrogen adsorption were then determined. Temperature-programmed reduction (TPR) measurements were carried out in a conventional flow system with a moisture trap connected to a TCD at temperatures ranging from room temperature to 900 °C with a heating rate of 5 °C/min. For the TPR measurements, a mixed stream of H_2 (2 ml/min) and Ar (20 ml/min) was used for 0.1 g of catalyst sample.

2.3. Hydrodechlorination of 1,1,2-trichloroethane

The hydrodechlorination of 1,1,2-trichloroethane into vinyl chloride monomer (VCM) was carried out in a continuous flow fixed-bed reactor at an atmospheric pressure. Each catalyst (0.2 g) with a size of 150–200 μm was charged into a tubular quartz reactor, and the catalyst was activated with a mixed stream of H_2 (20 ml/min) and N_2 (20 ml/min) at 500 °C for 6 h. The reaction temperature was maintained at 300 °C. TCE (7.28×10^{-3} mol/h) was sufficiently vaporized by passing a pre-heating zone and fed into the reactor continuously together with nitrogen carrier (20 ml/min). The products were periodically sampled, and analyzed with GC-MS and GC (HP 5890 II, FID). The catalytic reactions were carried out several times for each catalyst under the same conditions. In each run, TCE conversion and VCM selectivity were within the error range of $\pm 2\%$. TCE conversion and product selectivity were calculated on the basis of carbon balance. A relative activity (r/r_0), defined as the ratio of catalytic activity with respect to initial activity was measured to investigate the deactivation behavior of supported Ni catalysts.

3. Results and discussion

3.1. Textural properties of support and supported nickel catalysts

Textural properties of γ-Al_2O_3 and supported nickel catalysts are summarized in Table 1. Surface area of the supported nickel catalyst was smaller than that of the bare alumina support, whereas pore volume of the supported nickel catalyst was larger than that of the bare alumina support. The commercially available alumina support used in this work consists of non-porous nanoparticles, and its low pore volume is due to the pores formed by some aggregates of these nanoparticles. On the other hand, nickel species played a role of chemical glue for alumina particles in the supported catalysts [34]; a large number of pores were formed in the supported catalysts by the action of chemical

Table 1
Textural properties of γ-Al_2O_3 and supported nickel catalysts

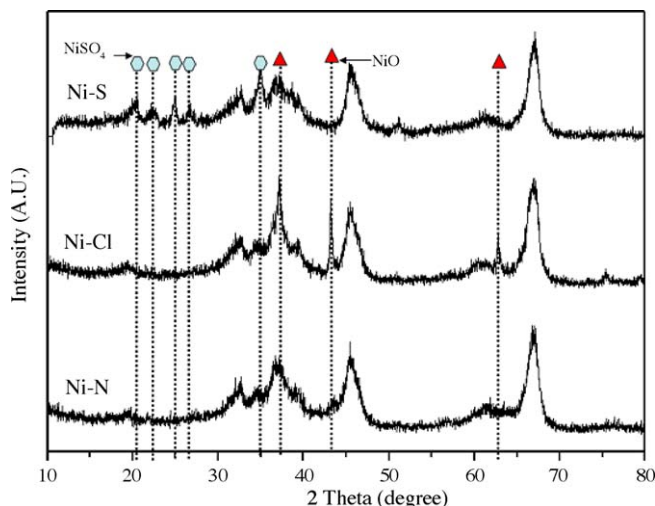|	γ-Al_2O_3	Ni-N	Ni-Cl	Ni-S
Surface area (m^2/g)	103	91	91	72
Pore volume (cm^3/g)	0.12	0.27	0.23	0.19
Nickel loading (%)	–	8.8	8.7	8.4
Nickel dispersion (%)	–	11.7	8.4	6.2

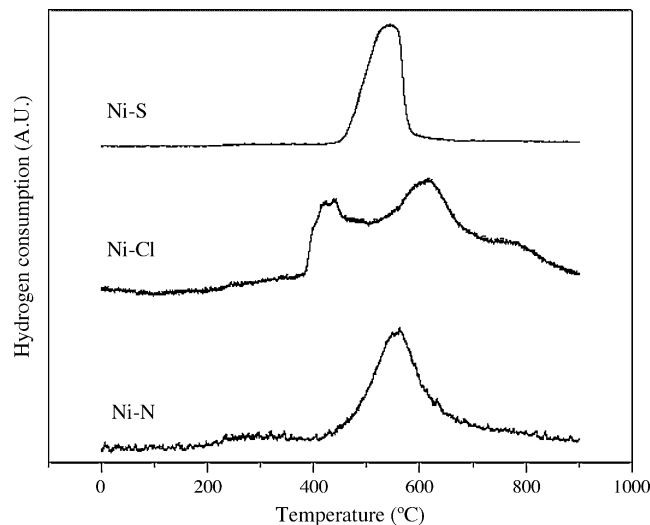Fig. 1. XRD patterns of supported Ni catalysts after calcination.

Fig. 2. TPR profiles of supported Ni catalysts.

glue. The surface areas and pore volumes of the supported catalysts were slightly different depending on the identity of nickel precursor.

3.2. Characteristics of supported nickel catalysts

Fig. 1 shows the XRD patterns of supported Ni catalysts after calcination. The Ni-N catalyst showed a typical XRD pattern for nickel catalyst supported on γ-Al_2O_3 without any peaks corresponding to nickel oxide, indicating relatively high dispersion of Ni species on the alumina support. On the other hand, the characteristic XRD peaks of nickel oxide were clearly observed in the Ni-Cl catalyst, indicating the formation of large nickel oxide particles. It is known that a sulfate group, relative to nitrate and chloride, is not completely removed at moderate calcination temperatures due to its strong interaction with the metal [35,36]. Under our experimental conditions, the sulfate group of nickel sulfate precursor was not completely removed as shown in Fig. 1, where the characteristic peaks of nickel sulfate were clearly seen in the XRD pattern of Ni-S catalyst. The presence of sulfate group was also confirmed from XPS measurements by observing the spectrum of the S 2p level. On the other hand, no peaks related to Cl and NO_3 were observed in the XPS spectra of Ni-Cl and Ni-N catalysts, respectively. This suggests that the chloride and nitrate ligands were completely removed by the calcination.

To investigate reducibility and metal-support interaction, TPR experiments were carried out. It is known that supported nickel catalysts show different reduction patterns depending on the nature of interaction between nickel and alumina support [37–42]. Bulk nickel oxide that does not interact with support is reduced at around 400 °C. When nickel is supported on γ-Al_2O_3, the interaction between metal and support decreases the susceptibility for nickel ion to be reduced to metallic nickel and its reduction peak appears within a temperature range of 500–700 °C. As shown in Fig. 2, the Ni-N catalyst exhibited a reduction peak at around 570 °C, a typical reduction pattern of Ni/γ-Al_2O_3 catalyst prepared using nickel nitrate precursor. The reduction peak of the Ni-S catalyst shifted to a slightly

lower temperature than that of the Ni-N catalyst, indicating a weaker interaction between Ni species and alumina support in the Ni-S catalyst. As mentioned earlier, the sulfate group interacted strongly with nickel, and therefore, it was not completely removed by the calcination. It is expected that the strong interaction between Ni and sulfate group would give rise to a weak interaction between Ni and alumina support. The Ni-Cl catalyst showed three TPR peaks at around 400, 600 and 780 °C. The peak at 400 °C can be assigned to the reduction of bulk nickel oxide, and the peak at around 600 °C can be attributed to the reduction of Ni ions that interacted strongly with the alumina support. When nickel ions are incorporated into alumina support or decorated by aluminum ions, the reduction peak is expected to occur at high temperature due to the formation of surface nickel aluminate-like species [43]. Therefore, the peak at around 780 °C in the Ni-Cl catalyst can be attributed to the reduction of nickel aluminate-like species.

The identity of nickel species on the alumina support was also confirmed by UV-DRS measurements. Fig. 3 shows the UV-DRS profiles of supported Ni catalysts. The bands at 715 and 377 nm represent the octahedrally coordinated Ni^{2+} species in the NiO lattice, while those in the range of 600–640 and 430 nm correspond to tetrahedrally coordinated Ni^{2+} species in the nickel aluminate lattice [44–46]. Both the bands related to NiO and nickel aluminate are relatively strong in the Ni-Cl catalyst, in good agreement with the TPR results. On the other hand, the Ni-S catalyst shows a band at 430 nm, the same position as the absorption band of the Ni^{2+} species in the nickel aluminate lattice. In the TPR pattern of the Ni-S catalyst, however, no reduction band for nickel aluminate was observed. Therefore, it is reasonable to conclude that the absorption band at 430 nm is closely related to octahedrally coordinated Ni^{2+} species that strongly interacted with sulfate group.

Fig. 4 shows the XRD patterns of reduced catalysts. The Ni-Cl catalyst exhibits sharp and narrow peaks for metallic Ni, while the Ni-N and Ni-S catalysts show small and broad peaks for metallic Ni, indicating the presence of large Ni particles in the Ni-Cl, compared to the Ni-N and Ni-S. This observation is in
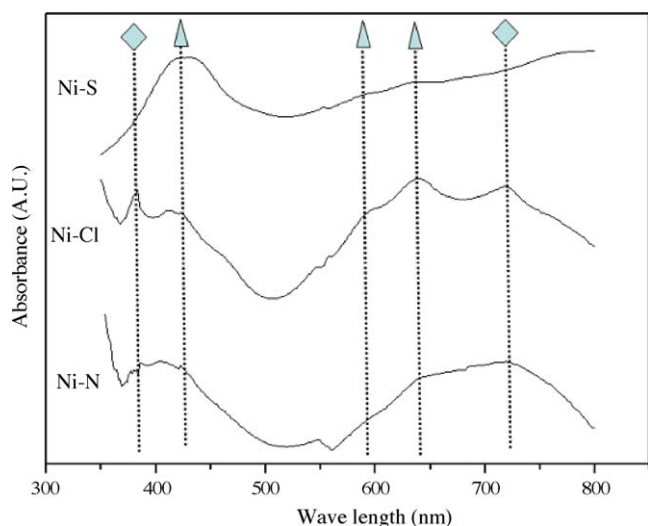
Fig. 3. UV-DRS profiles of supported Ni catalysts ((□) octahedral Ni ion in NiO lattice; (▲) tetrahedral Ni ion in NiAl$_2$O$_4$ lattice).

Fig. 5. XPS spectra of reduced Ni catalysts for Al 2p level.

good agreement with the TPR result in the sense that the Ni-Cl catalyst exhibited the low temperature reduction peak, which was assigned to the reduction of bulk nickel oxide. Since the temperature applied in the catalyst pretreatment was higher than the reduction temperature of bulk nickel oxide, it can be inferred that the large Ni particles in the Ni-Cl catalyst resulted from the reduction of bulk nickel oxide. In the case of the Ni-S catalyst, the characteristic peaks of nickel sulfate disappeared after reduction.

XPS spectra of reduced catalysts for Al 2p level showed a single peak at 74.4 eV (Fig. 5). In addition, the full width at half maximum (FWHM) value of Al 2p peak of the Ni-S catalyst was almost identical to that of the Ni-N catalyst in which the nitrate had been completely removed after calcination. This result reflects that Al in the Ni-S catalyst was not affected by sulfur species during the reduction, suggesting that residual sulfur species in the reduced Ni-S catalyst interacted strongly with nickel species, but not with Al. This results in the transformation of nickel sulfate into nickel sulfide [47]. Elemental analyses revealed that the sulfur content of the reduced Ni-S catalyst was
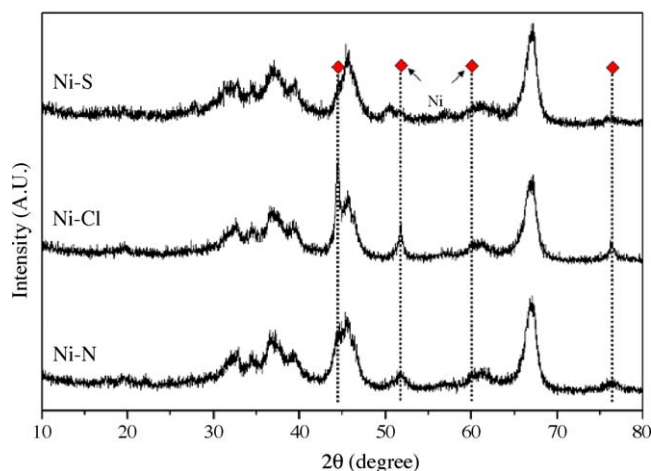
2.6 wt.%, slightly lower than that of the calcined Ni-S catalyst (3.5 wt.%).

3.3. Catalytic performance and catalyst deactivation

Fig. 6(a and b) show the TCE conversion, relative activity, VCM selectivity, and VCM yield as a function of reaction time at 300 °C. The hydrodechlorination of TCE produces HCl and various chlorinated hydrocarbons. In the catalytic reaction, VCM and ethylene were the main products. It was observed that VCM selectivity was increased with decreasing TCE conversion. Scheme 1 shows the suggested reaction mechanism for the hydrodechlorination of TCE. It is known that the hydrodechlorination of TCE occurs via sequential removal of chlorine species, which results from C–Cl bond cleavage [14–16]. VCM is formed as a reaction intermediate. The initial TCE conversion was highest over the Ni-N catalyst and lowest over the Ni-S catalyst. The difference in initial conversion between the catalysts can be explained by the metal dispersion, as listed in Table 1. Judging from the hydrodechlorination mechanism proposed by many investigators [7,12,15,17,18], the adsorption of hydrogen on the catalyst surface is prerequisite for the initiation of hydrodechlorination. Compared to the Ni-Cl and Ni-S catalysts, the Ni-N catalyst retained high metal dispersion. This indicates that the Ni-N catalyst has much more chance of initial catalytic reaction. On the other hand, the Ni-N catalyst experienced a drastic catalyst deactivation. As mentioned earlier, catalyst deactivation in the hydrodechlorination is mainly due to two factors. One is the coke deposition [20–22] and the other is the interaction between HCl and metallic phase that leads to the formation of inactive metal chloride [12,18,23–27].

To investigate the effect of coke deposition on the catalyst deactivation, the hydrodechlorination of TCE was carried out over the Ni/SiO$_2$ (the results are not shown here). Compared to the Ni/Al$_2$O$_3$ catalyst, the amount of coke deposited on the Ni/SiO$_2$ catalyst was negligible. However, Ni/SiO$_2$ catalyst experienced severe catalyst deactivation. Although different

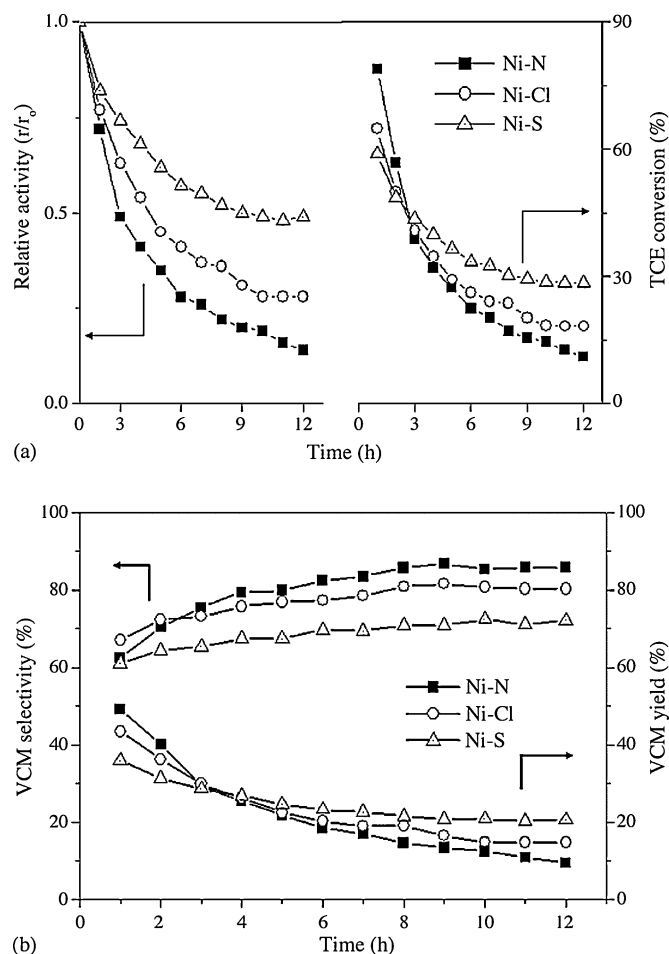Fig. 4. XRD patterns of reduced Ni catalysts.

(a)

(b)

Fig. 6. TCE conversion, relative activity, VCM selectivity, and VCM yield as a function of reaction time at 300 °C.

metal-support interactions can also affect the catalytic performance, the above result implies that coke deposition is not a major factor for catalyst deactivation in this reaction. Compared to the Ni-N catalyst, the Ni-S and Ni-Cl catalysts experienced rather mild catalyst deactivation. It has been reported that surface metal species such as metal hydrosilicate and metal aluminate are capable of enhancing the catalyst stability toward catalyst deactivation [14,48]. In addition, it has also been observed that catalyst deactivation could be reduced by increasing the metal particle size [14,49]. From these viewpoints, it is expected that large nickel particles together with nickel aluminate species in the Ni-Cl catalyst retarded the catalyst deactivation, as evidenced by TPR and XRD analyses.

The greatest tolerance against the catalyst deactivation was observed in the Ni-S catalyst. To elucidate the deactivation-resistant properties of Ni-S catalyst, XPS analyses of the used

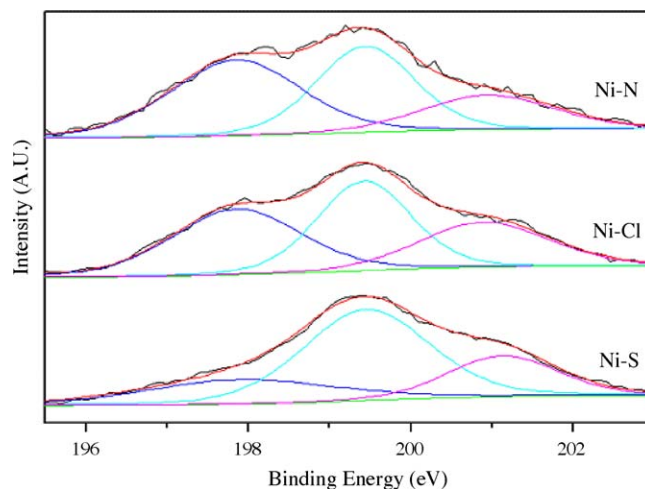Scheme 1. Reaction mechanism for the hydrodechlorination of TCE.

Fig. 7. XPS spectra of supported Ni catalysts for Cl 2p level after 12 h-reaction.

Table 2
Binding energy and binding energy contribution of Cl 2p level after deconvolution

	Binding energy (contribution)		
Ni-N	198.2 eV (44.4%)	199.6 eV (34.9%)	200.9 eV (20.7%)
Ni-Cl	198.3 eV (37.3%)	199.8 eV (37.4%)	200.9 eV (25.3%)
Ni-S	198.2 eV (22.6%)	199.8 eV (55.7%)	201.1 eV (21.8%)

catalysts were carried out. Differences in interaction between chlorine species and catalysts were clearly observed from XPS measurements for the Cl 2p level, as shown in Fig. 7. The XPS spectra of used catalysts for the Cl 2p level showed three spin-orbit doublets at around 198.2, 199.8 and 200.9 eV. The component of the lowest binding energy can be assigned to the binding energy of Cl^- anion, while the others correspond to covalent chlorine species, i.e., covalent chlorocarbon (C–Cl) [50–53]. Considering that the catalyst deactivation in the hydrodechlorination mainly originates from the interaction between HCl and metallic phase, the lowest binding energy may be more closely related to the catalyst deactivation than the others. The contribution of each component to the binding energy is summarized in Table 2. Compared to the Ni-N and Ni-Cl catalysts, the Ni-S catalyst showed a relatively low portion of the lowest binding energy, implying more tolerant behavior toward catalyst deactivation. As mentioned before, the Ni-S catalyst retained finely dispersed nickel sulfide after reduction. Although the sulfur species may prohibit the adsorption of hydrogen on nickel surface and lead to a lower dispersion, it can serve as a barrier to strong interaction between HCl and metallic nickel. In addition, it has been reported that the nickel sulfide itself has catalytic activity for hydrodechlorination [54]. Therefore, it is reasonable to expect that the Ni-S catalyst would exhibit the most stable catalytic activity in the hydrodechlorination of TCE.

4. Conclusions

Supported Ni catalysts on γ-Al$_2$O$_3$ were prepared using different nickel precursors, nickel nitrate (Ni-N), nickel chlo-

ride (Ni-Cl), and nickel sulfate (Ni-S). The supported catalysts showed different catalytic properties such as reducibility, metal-support interaction, and metal dispersion. The Ni-N catalyst exhibited the highest initial activity. However, it experienced severe catalyst deactivation and showed the lowest catalytic performance in the long run. On the other hand, the Ni-Cl and Ni-S catalysts showed a relatively stable catalytic performance, because large nickel particles with a nickel aluminate structure in the Ni-Cl catalyst and highly dispersed sulfur species in the Ni-S catalyst prevented strong interaction between HCl and metallic nickel. It was also revealed that the sulfur species in the Ni-S catalyst were very effective in retarding the catalyst deactivation. Among the catalysts tested, the Ni-S catalyst experienced the lowest catalyst deactivation and showed the highest VCM yield after a period of catalytic reaction.
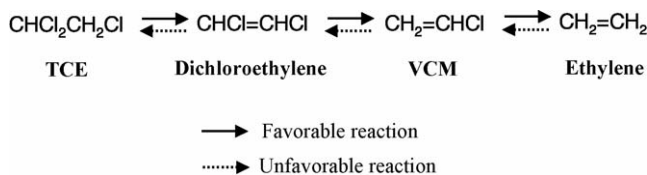
Acknowledgements

References

[1] F.S. Rowland, M.J. Molina, Nature 249 (1974) 810.
[2] W. Brune, Nature 379 (1996) 486.
[3] R.B. Lapierre, L. Guczi, W.L. Kranich, A.H. Weiss, J. Catal. 52 (1978) 230.
[4] H.R. Buser, Chemosphere 8 (1979) 415.
[5] B.F. Hagh, D.T. Allen, Chem. Eng. Sci. 45 (1990) 2695.
[6] J. Stach, V. Pekarek, R. Endrst, J. Hetflejs, Chemosphere 39 (1999) 2391.
[7] G. Tavoulais, M.A. Keane, J. Mol. Catal. A 142 (1999) 187.
[8] P. Kim, Y. Kim, C. Kim, H. Kim, Y. Park, J.H. Lee, I.K. Song, J. Yi, Catal. Lett. 89 (2003) 185.
[9] J.K. Murthy, S.C. Shekar, V.S. Kumar, B.D. Raju, B. Sreedhar, P.S.S. Prasad, P.K. Rao, K.S.R. Rao, F.J. Berry, L.E. Smart, J. Mol. Catal. A 223 (2004) 347.
[10] W. Wu, J. Xu, Catal. Commun. 5 (2004) 591.
[11] P. Kim, Y. Kim, H. Kim, I.K. Song, J. Yi, J. Mol. Catal. A 219 (2004) 87.
[12] G. Yuan, M.A. Keane, J. Catal. 225 (2004) 510.
[13] V.I. Kovalchuk, J.L. d'Itri, Appl. Catal. A 271 (2004) 13.
[14] Y.H. Choi, W.Y. Lee, Catal. Lett. 67 (2000) 155.
[15] Y.H. Choi, W.Y. Lee, J. Mol. Catal. A 174 (2001) 193.
[16] Y. Park, T. Kang, J. Lee, P. Kim, H. Kim, J. Yi, Catal. Today 97 (2004) 195.
[17] M.K. Keane, G. Pina, G. Tavoularis, Appl. Catal. B 48 (2004) 275.
[18] K.V. Murthy, P.M. Patlerson, G. Jacobs, B.H. Davis, M.A. Keane, J. Catal. 223 (2004) 74.
[19] E.J. Creyghton, M.H.W. Burgers, J.C. Jansen, H. van Bekkum, Appl. Catal. A 128 (1995) 275.
[20] M.L. Jarzyna, A. Srebowata, W. Juszczyk, Z. Karpinski, J. Mol. Catal. A 224 (2004) 171.
[21] V. de Jong, R. Louw, Appl. Catal. A 271 (2004) 153.
[22] G. Yuan, M.A. Keane, Catal. Today 88 (2003) 27.
[23] R. Gopinath, N. Lingaiah, B. Sreedhar, I. Suryanarayana, P.S.S. Prasad, A. Obuchi, Appl. Catal. B 46 (2003) 587.
[24] Y. Cesteros, P. Salagre, F. Medina, J.E. Sueiras, D. Tichit, B. Coq, Appl. Catal. B 32 (2001) 25.
[25] M. Martino, R. Rosal, H. Sastre, F.V. Diez, Appl. Catal. B 20 (1999) 301.
[26] E.-J. Shin, M.A. Keane, Appl. Catal. B 18 (1998) 241.
[27] G.D. Angel, J.L. Benitez, J. Mol. Catal. A 165 (2001) 9.
[28] L. Chen, T. Horiuchi, T. Mori, Appl. Catal. A 209 (2001) 97.
[29] C. Perego, P. Villa, Catal. Today 34 (1997) 281.
[30] G. Cocco, R. Canpostrini, M.A. Cabras, G. Carturan, J. Mol. Catal. A 94 (1994) 299.
[31] S. Yoshinaka, K. Segawa, Catal. Today 45 (1998) 293.
[32] H. Kusana, K.K. Bando, K. Okabe, H. Arakawa, Appl. Catal. A 205 (2001) 285.
[33] S. Wang, G.Q. Lu, Appl. Catal. A 169 (1998) 271.
[34] P. Kim, Y. Kim, H. Kim, I.K. Song, J. Yi, Appl. Catal. A 272 (2004) 157.
[35] Y. Zhan, C. Yin, C. Zhang, W. Wang, G. Wang, J. Solid State Chem. 117 (2004) 2281.
[36] J.R. Sohn, W.C. Park, Appl. Catal. A 239 (2003) 269.
[37] J. Zielinski, J. Catal. 76 (1982) 157.
[38] G.R. Gavalas, C. Phichitkul, G.E. Voecks, J. Catal. 88 (1984) 54.
[39] P.K. De Bokx, W.B.A. Wassenberg, J.W. Geus, J. Catal. 104 (1987) 86.
[40] J.M. Rynkowski, T. Paryjczak, M. Lenik, Appl. Catal. A 106 (1992) 73.
[41] O. Dewaele, G.F. Froment, J. Catal. 184 (1999) 499.
[42] B.W. Hoffer, A.D. Langeveld, J.P. Janssens, R.L.C. Bonne, C.M. Lok, J.A. Moulijn, J. Catal. 192 (2000) 432.
[43] R. Lanber, G. Schulz-Ekloff, J. Catal. 146 (1994) 601.
[44] M.L. Jocomo, M. Schiavello, A. Cimino, J. Phys. Chem. 75 (1971) 1034.
[45] B. Vos, E. Poels, A. Blick, J. Catal. 77 (2001) 198.
[46] K.M. Lee, W.Y. Lee, Catal. Lett. 83 (2002) 65.
[47] C.F. Ng, S. Shan, S.Y. Lai, Appl. Catal. A 16 (1998) 209.
[48] Y.S. Cho, J.C. Park, B. Lee, Y. Kim, J. Yi, Catal. Lett. 81 (2002) 89.
[49] Z.C. Zhang, B.C. Beard, Appl. Catal. A 174 (1998) 33.
[50] S. Ntais, V. Dracopoulos, A. Siokou, J. Mol. Catal. A 220 (2004) 199.
[51] L.H. Bloxham, S. Hag, Y. Yugnet, J.C. Bertolini, R. Raval, J. Catal. 227 (2004) 33.
[52] J.L. Gautier, J.F. Marco, M. Gracia, J.R. Gancedo, V. de la, G. Guadar-rama, H. Nguyen-Cong, P. Chartier, Electrochim. Acta 48 (2002) 199.
[53] L.M. Go'mez-Sainero, X.L. Seoane, J.L.G. Fierro, A. Arcoya, J. Catal. 209 (2002) 279.
[54] J. Frimmel, M. Zdrazil, J. Catal. 167 (1997) 286.